

# Soliton Crystals in Kerr Microresonator Frequency Combs

Daniel C. Cole<sup>1</sup>, Erin S. Lamb<sup>1</sup>, Pascal Del’Haye<sup>1,2</sup>, Scott A. Diddams<sup>1</sup>, and Scott B. Papp<sup>1</sup>

<sup>1</sup>National Institute of Standards and Technology (NIST), Boulder, CO 80305, USA

<sup>2</sup>Present address: National Physical Laboratory (NPL), Teddington, TW11 0LW, United Kingdom

Corresponding author: daniel.cole@nist.gov

**Abstract:** We explore ordered soliton ensembles in Kerr microresonators. These soliton crystals are stabilized through collective soliton interactions mediated by defects in resonator mode structure, and require only adiabatic tuning of the pump for generation.

**OCIS codes:** (190.5530) Pulse propagation and temporal solitons; (140.3945) Microcavities

Dissipative Kerr-cavity solitons are a promising candidate for chip-compatible generation of optical frequency combs (“microcombs”). These solitons have been reported in several material platforms, and have begun to meet requirements for performing optical frequency metrology: They can be generated with spectra broad enough for self-referencing through dispersive-wave generation [1], externally broadened to span 2/3 octave or octave bandwidth [2,3], and efficiently operated with high stability for long measurement runs [4]. Demonstrations of solitons in microcombs have largely focused on single- or few-soliton states, for which generation is complicated by cavity thermal stability effects. To support solitons, the pump laser must be red-detuned with respect to the linear cavity resonance frequency, shifted by thermo-optic effects [5]. While solitons do counterbalance the thermal instability caused by a red-detuned continuous-wave pump laser, a challenge exists in achieving this balance in the  $\mu$ s to ms thermal timescale of microresonators [6–8]. Techniques to stabilize single Kerr solitons include pump frequency tuning [7], power kicking [1,4], and heater tuning of the cavity resonance [9].

In this paper, we comprehensively explore the creation of Kerr-cavity soliton crystals in which an ensemble of single solitons entirely fills the cavity and becomes collectively ordered. These soliton crystals offer an operational efficiency since they evolve adiabatically from blue-detuned, thermally stable Kerr microcombs. Here the ensemble of many solitons has an average intracavity power similar to that of a blue-detuned microcomb, hence a steady thermal frequency shift of the cavity persists in the evolution from blue-to-red detuning and soliton-crystal formation. A second aspect of our study pertains to the distinctive optical spectra and discrete steps in spectral phase of soliton crystals [10,11], which manifest from the precise, collective order of the soliton-crystal pulse train. We show how defects (or avoided mode-crossings) in the microresonator mode structure induce crystallization of a multi-soliton ensemble, leading to collective organization in which many co-propagating solitons populate a uniform crystalline grid in the cavity.

Our experimental system for the generation of soliton crystals, shown schematically in Fig. 1a, consists of a silica resonator into which a tunable telecommunications-band continuous-wave (CW) pump laser is coupled by a tapered optical fiber. When the pump laser frequency is decreased across the resonance and then held at fixed red detuning, a soliton crystal can be generated. In Figs. 1b and 1c, we plot an example of a soliton crystal generated in a silica disk resonator with 16.5 GHz FSR [12]. Along with the experimental spectrum (black), we plot simulations of the crystal’s spectrum, intensity, and spectral phase (blue). This crystal is composed of 23 pulses, each of which is the same fundamental single soliton solution to the Lugiato-Lefever equation (LLE), which describes the evolution of the intracavity field in Kerr microcombs and is used for simulations in this paper. The 23 pulses are spaced by  $2\pi/24$  radians in the azimuthal coordinate  $\theta$ —the resulting hole in the pulse train leads to the characteristic *primary-comb-plus-soliton* nature of the spectrum shown in Fig. 1c. As they are all shifted copies of

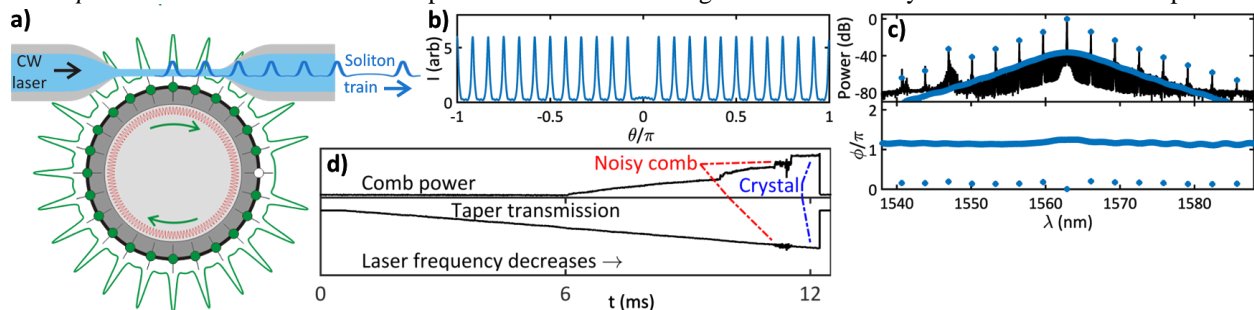


Fig. 1. (a) Schematic depiction of the experiment. The oscillating background that stabilizes the soliton crystal is shown in red. (b) Simulated intensity of a crystal with 23 pulses spaced by  $2\pi/24$ . (c) Experimental and simulated spectra, and simulated phases, corresponding to the crystal shown in (b). (d) Plots of the taper transmission and comb power across a laser sweep that generates a soliton crystal.

the same soliton, the pulses co-propagate at the group velocity, leading to translation of the crystal around the disk.

Key to the generation of these soliton crystals is the correspondence between the intracavity power, and thus the resonator steady-state thermo-optic frequency shift, of the crystal and the noisy comb which precedes it. In Fig. 1d we plot measurements of the taper transmission (essentially an inverted intracavity power measurement) and the power converted from the pump laser to other frequency components of the comb. The crystal corresponds to the flat pedestal at the end of the comb power trace. The plot of the taper transmission shows that there is a negligible change in average intracavity power upon generation of the crystal, and there is an increase in frequency conversion from the pump to other comb modes. The presence of a noisy comb can be seen in both traces as fluctuations preceding crystal formation. To generate a long-lived crystal, the laser scan is stopped on the flat pedestal in the comb power trace corresponding to the crystal.

An important feature of soliton crystals is that the pulses are arranged with uniform, or nearly uniform, relative separations, which gives rise to the prominent “primary comb” lines seen in the spectrum in Fig. 1c. The LLE, which describes single- and few-soliton states, provides no mechanism that we are aware of to induce this crystallization. We propose that it arises from soliton interactions mediated by resonator mode-structure defects. The model is this: An avoided mode crossing due to coupling with a different spatial mode family locally shifts the resonator’s modes [13], which enhances comb generation on modes which are shifted closer to the equidistant frequency-domain grid defined by the comb’s repetition rate. This results in excess power in one or more comb modes. The excess power interferes with CW laser power in the cavity, leading to an oscillation at the difference frequency of the pump and the affected comb mode [14]. This phenomenon also occurs for bichromatically-pumped microcombs, where it has been theoretically shown that solitons preferentially exist at the peaks of the oscillation [15]. In this way, the oscillating background provides for a discrete set of allowed angular separations between pulses circulating in the cavity. To carry out the simulations in this paper, we have perturbed the LLE to account for the mode-structure defects associated with avoided mode-crossings visible in the experimental spectra.

In Figs. 2a-f, we plot two different soliton crystals. The 24-soliton crystal plotted in Figs. 2a and 2b is similar to the crystal plotted in Figs. 1c-d, but with a soliton shifted rather than dropped, giving rise to the broad lobes in the optical spectrum. The periodicity of the lobes is highly sensitive to the magnitude of the shift of this pulse’s position. A simulation of the crystal indicates that the shift is  $2 \cdot 2\pi / (7 \cdot 24)$  radians—precisely what would arise from shifting the pulse by two periods of the interference between mode  $7 \cdot 24 = 168$  and the CW background. In Fig. 2c, we plot the perturbation to the resonator mode structure that is used to simulate this crystal (blue dots), along with second-order dispersion for comparison (orange curve). Here,  $\alpha$  is the mode-dependent detuning between comb mode and resonator mode in units of half the resonance linewidth, and is positive for red detuning. A logarithmic-scale plot of the simulated intensity is shown in Fig. 1d, in which the oscillating background is visible. This oscillation arises from the avoided mode-crossing, and in turn gives rise to soliton crystallization.

Figs. 2e-f depict a soliton crystal generated in a silica rod resonator with 25 GHz FSR [16]. An avoided mode-crossing enhances comb generation on mode 49, leading to an oscillating background in the cavity with a period of  $2\pi/49$  radians. In this case, it is not possible for the pulses to arrange themselves on a uniform grid. A grid with 7 pulses spaced by  $7 \cdot 2\pi/49$  is incompatible with the dynamics of the comb generation—the noisy comb preceding the generation of the crystal fills the resonator too densely for only 7 pulses to be generated. Instead, 16 pulses are generated, with 15 pairs spaced by  $3 \cdot 2\pi/49$  and one pair spaced by  $4 \cdot 2\pi/49$ . This is a uniformly spaced crystal whose spacing is contracted relative to the nearest integer fraction of the round trip time, which is  $T_{RT}/16$ . This contraction gives rise to the catenary-like spectral features, and is necessitated by the fact that the solitons must exist at the peaks of the oscillating background coming from the avoided mode crossing.

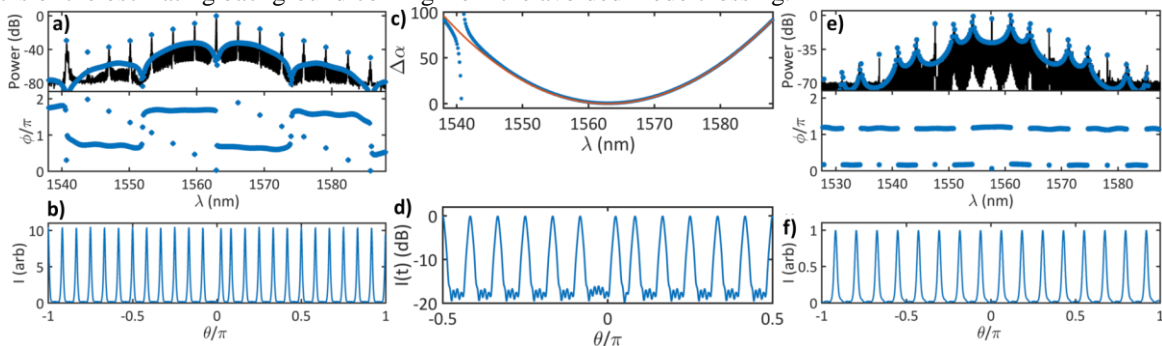


Fig. 2. (a-b) Experimental spectrum and simulated spectrum, phases, and intensity of a crystal with 24 pulses, with one pulse shifted from uniform spacing. (c) Perturbed resonator mode-structure which stabilizes the crystal. (d) Log-scale plot of the intensity shown in (b), with the oscillating background visible. (e-f) Experimental spectrum and simulated spectrum, phases, and intensity of a crystal with 16 pulses, with spacing that is slightly contracted relative to uniform spacing by  $2\pi/16$ , as required by the position of the avoided mode-crossing.

We confirm this simple model of the experimental spectra as superpositions of solitons by making time-domain auto- and cross-correlation measurements, shown in Figure 3. Here we work with the crystal plotted in Figs. 1b-c and again in Fig. 3a. We generate a reference pulse by sending the pulse train through a spatial light modulator and attenuating the pump component and the four most prominent comb lines – the effect of this attenuation is shown by the simulated red spectrum. An autocorrelation of the reference pulse is shown in black in Fig. 3b, along with a calculation from the waveform corresponding to the red spectrum in Fig. 3a (red). The result of a cross-correlation measurement between the reference pulse and the soliton crystal is plotted in black in Fig. 3c. To understand the shape of the measured cross-correlation, the pump light which is transmitted past the resonator through the tapered fiber must be taken into account. This increases the amplitude of the pump component in the optical spectrum, and shifts its phase relative to the rest of the comb. A simulated cross-correlation with these effects included is plotted in green in Fig. 3c, and we find good agreement with the measurement.

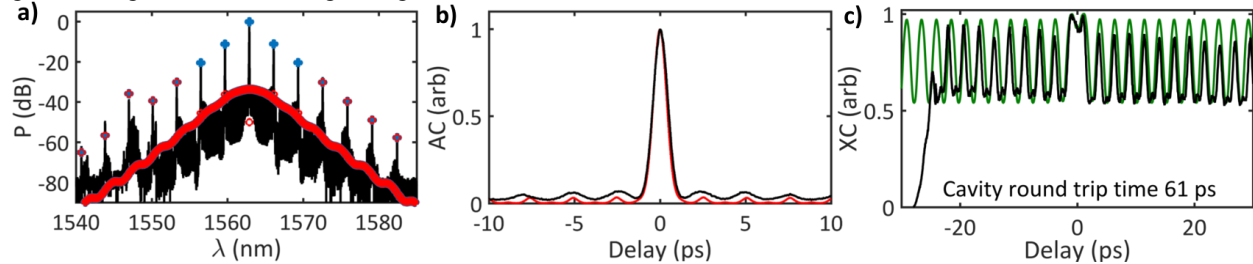


Fig. 3 (a) Experimental (black) and simulated (blue) spectrum of a soliton crystal, and spectrum with attenuation applied for generation of a reference pulse (red). (b) Measured (black) and calculated (red) autocorrelations of the reference pulse resulting from applying the attenuation mask to the spectrum of the crystal. (c) Measured (black) and simulated (green) cross-correlations between the reference pulse and the pulse train.

The observation and modeling of these soliton crystals provides evidence for new soliton behavior in microcombs which goes beyond the standard LLE. Additionally, the crystals contrast with single- and few-soliton states in that they are adiabatically accessible, providing a simpler route for soliton generation in microcombs. These pulse trains can subsequently be shaped into single pulses by applying a deterministic attenuation mask, as seen in Figs. 3a and 3b. Microcombs continue to reveal rich, novel physics and suggest new routes to applications.

The authors gratefully acknowledge fabrication of the silica disk resonators by Ki Youl Yang and Kerry Vahala.

This material is based upon work supported by the Air Force Office of Scientific Research, DARPA QuASAR, NASA, NIST, NRC, and NSF-GRFP. This work is a contribution of the US government and is not subject to copyright in the United States.

- [1] V. Brasch, T. Herr, M. Geiselmann, G. Lihachev, M. H. P. Pfeiffer, M. L. Gorodetsky, and T. J. Kippenberg, "Photonic chip-based optical frequency comb using soliton Cherenkov radiation," *Science* **351**, 357 (2016).
- [2] P. Del'Haye, A. Coillet, T. Fortier, K. Beha, D. C. Cole, K. Y. Yang, H. Lee, K. J. Vahala, S. B. Papp, and S. A. Diddams, "Phase Coherent Link of an Atomic Clock to a Self-Referenced Microresonator Frequency Comb," arXiv 1511.08103 (2015).
- [3] J. D. Jost, T. Herr, C. Lecaplain, V. Brasch, M. H. P. Pfeiffer, and T. J. Kippenberg, "Counting the cycles of light using a self-referenced optical microresonator," *Optica* **2**, 706–711 (2015).
- [4] X. Yi, Q.-F. Yang, K. Y. Yang, M.-G. Suh, and K. Vahala, "Soliton frequency comb at microwave rates in a high-Q silica microresonator," *Optica* **2**, 1078–1085 (2015).
- [5] C. Godey, I. V. Balakireva, A. Coillet, and Y. K. Chembo, "Stability analysis of the spatiotemporal Lugiato-Lefever model for Kerr optical frequency combs in the anomalous and normal dispersion regimes," *Phys. Rev. A* **89**, 063814 (2014).
- [6] S. Coen and M. Erkintalo, "Universal scaling laws of Kerr frequency combs," *Opt. Lett.* **38**, 1790–2 (2013).
- [7] T. Herr, V. Brasch, J. D. Jost, C. Y. Wang, N. M. Kondratiev, M. L. Gorodetsky, and T. J. Kippenberg, "Temporal solitons in optical microresonators," *Nat. Photonics* **8**, 145–152 (2013).
- [8] T. Carmon, L. Yang, and K. J. Vahala, "Dynamical thermal behavior and thermal self-stability of microcavities," *Opt. Express* **12**, 4742–4750 (2004).
- [9] C. Joshi, J. K. Jang, K. Luke, X. Ji, S. A. Miller, A. Klenner, Y. Okawachi, M. Lipson, and A. L. Gaeta, "Thermally Controlled Comb Generation and Soliton Modelocking in Microresonators," arXiv 1603.08017 (2016).
- [10] P. Del'Haye, A. Coillet, W. Loh, K. Beha, S. B. Papp, and S. A. Diddams, "Phase steps and resonator detuning measurements in microresonator frequency combs," *Nat. Commun.* **6**, 5668 (2015).
- [11] P. Del'Haye, K. Beha, S. B. Papp, and S. A. Diddams, "Self-Injection Locking and Phase-Locked States in Microresonator-Based Optical Frequency Combs," *Phys. Rev. Lett.* **112**, 043905 (2014).
- [12] H. Lee, T. Chen, J. Li, K. Y. Yang, S. Jeon, O. Painter, and K. J. Vahala, "Chemically etched ultrahigh-Q wedge-resonator on a silicon chip," *Nat. Photonics* **6**, 369–373 (2012).
- [13] H. A. Haus and W. Huang, "Coupled-Mode Theory," *Proc. IEEE* **79**, 1505–1518 (1991).
- [14] T. Herr, V. Brasch, J. D. Jost, I. Mirgorodskiy, G. Lihachev, M. L. Gorodetsky, and T. J. Kippenberg, "Mode Spectrum and Temporal Soliton Formation in Optical Microresonators," *Phys. Rev. Lett.* **113**, 1–6 (2014).
- [15] T. Hansson and S. Wabnitz, "Bichromatically pumped microresonator frequency combs," *Phys. Rev. A - At. Mol. Opt. Phys.* **90**, 1–7 (2014).
- [16] P. Del'Haye, S. A. Diddams, and S. B. Papp, "Laser-machined ultra-high-Q microrod resonators for nonlinear optics," *Appl. Phys. Lett.* **102**, 221119 (2013).